RESEARCH PAPER

Shape and Property Guided Virtual Screening of the ZINC Database for Potential ABCB1 Inhibitors: Multiple Ligand Simultaneous Docking, Ensemble Docking, and Molecular Dynamics Simulations

Rupali M. Barhate [1,2 *], **Minal Ghante** [1], **Rajesh B. Patil** [2]

[1] Department of Pharmaceutical Chemistry, Sinhgad Technical Education Society's, Smt. Kashibai Navale College of Pharmacy, Kondhwa (Bk.), Savitribai Phule Pune University, Pune 411048, Maharashtra, India

[2] Department of Pharmaceutical Chemistry, Sinhgad Technical Education Society's, Sinhgad College of Pharmacy, Vadgaon (Bk.), Savitribai Phule Pune University,Pune 411041, Maharashtra, India

* Corresponding author: Rupali M. Barhate, rupali.barhate2020@gmail.com

Abstract

Cancer remains a major global health challenge, and the development of effective therapies is limited due to multidrug resistance. Overexpression of ATP-binding cassette subfamily B member 1 (ABCB1/P-glycoprotein), an ATP-dependent efflux transporter, contributes to anticancer such multidrug resistance by reducing intracellular drug accumulation. Although third-generation ABCB1 inhibitors such as zosuquidar has proven potent in vitro activity have limiting activity in a randomized phase III clinical trial, highlighting the need to identify alternative candidate inhibitors. This study is aimed to identify potential ABCB1 inhibitors from the ZINC20 database using an integrated shape and property guided virtual screening workflow, multiple-ligand simultaneous docking (MLSD), ensemble docking, and molecular dynamics (MD) simulations. Around 1.5 million compounds selected according to molecular weight and lipophilicity criteria from ZINC20 database based on zosuquidar features, and were further screened using 3D shape similarity and FCFP4-like Morgan fingerprints in VSFlow. Further physicochemical filtering based on hydrogen bond donors and acceptors, rotatable bonds, and topological polar surface area resulted in 826 hits. The hits were subjected to AutoDock Vina multi ligand simultaneous docking against human ABCB1 (PDB ID: 7A6F). Eighty two compounds, with comparably better binding affinities than zosuquidar were evaluated with ensemble docking against 23 ABCB1 conformations, generated from rotamerically induced perturbations with langevin dynamics (L-RIP) method. Four top ranked

hits were subjected to 100 ns transmembrane MD simulations in GROMACS and results were compared with zosuquidar. The hit molecules exhibited more favourable ensemble docking scores than zosuquidar, with ZINC001463799743 showing the best mean score (−17.44 ± 0.71 kcal mol^{-1} versus −15.03 ± 0.75 kcal mol^{-1}) across the receptor ensemble. ZINC001463799743 exhibited the lowest ligand RMSD (0.168 ± 0.019 nm), whereas ZINC000256027845 maintained the highest average hydrogen-bond count (1.65 ± 0.96). MM-GBSA analysis showed a more favourable binding free energy for ZINC000256027845 than for zosuquidar (−116.93 ± 7.57 versus −107.89 ± 3.41 kcal mol^{-1}). These findings identify computationally promising ABCB1 binding candidates which can be experimentally validated.

Keywords: ABCB1; P-glycoprotein; multidrug resistance; zosuquidar; ligand-based virtual screening; multiple ligand simultaneous docking; ensemble docking; molecular dynamics simulation; MM-GBSA

How to cite this article: Rupali M. Barhate 12 * Minal Ghante 1 Rajesh B. Patil 2. Shape and Property Guided Virtual Screening of the ZINC Database for Potential ABCB1 Inhibitors: Multiple Ligand Simultaneous Docking, Ensemble Docking, and Molecular Dynamics Simulations. Int J Drug Deliv Technol. 2026;16(87s):1828-1832. DOI: 10.25258/ijddt.16.87s.195.

Introduction

Cancer is a major global health challenge characterised by uncontrolled cell proliferation, tissue invasion, and, in malignant disease, the potential to metastasise to distant organs. Despite advances in early detection, molecularly targeted therapy, immunotherapy, and precision oncology, cancer remains a leading cause of morbidity and mortality worldwide. In 2022, approximately 20 million new cancer cases and 9.7 million cancer-related deaths were estimated globally, underscoring the continuing need for more effective therapeutic strategies [1]. Although several therapeutic interventions are available to improve the outcomes in several malignancies, resistance remains a major challenge. Here, resistance may arise through genetic and epigenetic alterations, activation of alternative signalling pathways, changes in drug targets, enhanced DNA repair, altered cell-death pathways, and reduced intracellular drug accumulation. Among these mechanisms, ATP-binding cassette (ABC) transporter mediated drug efflux is an important contributor to multidrug resistance (MDR) in serval tumors [2,3]. The human ABC transporter superfamily comprises 48 members classified into seven subfamilies (ABCA-ABCG) according to sequence and structural characteristics. These membrane proteins generally contain transmembrane domains (TMDs), which form the substrate translocation pathway, and nucleotide-binding domains (NBDs), which bind and hydrolyse ATP to drive transport [2,4]. ABC transporters are important in physiological functions, including the transport of endogenous molecules and the elimination of xenobiotics. However, this protective role is the concern in cancer chemotherapy when transporter overexpression or activity reduces intracellular drug concentrations below those required for effective cytotoxicity. Among these transporters, ABCB1, also known as P-glycoprotein (P-gp or MDR1), is one of the most

extensively studied mediators of drug efflux and treatment resistance. Physiologically expressed in tissues such as the intestine, liver, kidney, placenta, and blood brain barrier, ABCB1 restricts the absorption or tissue penetration of numerous clinically proven drugs. In malignant cells, its overexpression can reduce the intracellular accumulation of diverse anticancer agents, including anthracyclines, taxanes, and vinca alkaloids, thereby contributing to treatment failure [3–6]. A major challenge in developing ABCB1 inhibitors is the multi-specific and extended drug-binding cavity. The transmembrane drug binding region is large, conformationally adaptable, and predominantly lined by hydrophobic and aromatic residues inducing transport of chemically diverse substrates without a single conserved pharmacophore [5,6]. Structural and biochemical investigations reported suggest that the transporter accommodates ligands through a combination of hydrophobic contacts, aromatic interactions, and ligand-induced rearrangements of its transmembrane helices [7,8]. The reports also suggest that the cysteine cross linking experiments two different drug molecules can bind simultaneously within the ABCB1 drug-binding region, occupying distinct sites [9]. The structural studies further revealed paired occupancy by inhibitors such as elacridar, tariquidar, and zosuquidar in particular inhibitor bound conformations of human ABCB1 [8]. Especially, the structure of a human mouse chimeric transporter highlights the binding of two zosuquidar molecules within the drug binding region [10]. The previous reports resulted in the development of three generations of ABCB1 inhibitors [2,11]. First generation modulators, including verapamil, were existing therapeutic agents found to inhibit drug efflux, but their pharmacological activities are limited due to the concentrations that could be safely administered. Second generation agents, including valspodar, were developed to improve inhibitory potency, but have limiting efficacy [12,13]. Third-generation inhibitors, including tariquidar, elacridar, laniquidar, and zosuquidar, were designed to achieve greater potency and selectivity with fewer pharmacokinetic interactions [11,14–17]. However, their clinical efficiency has remained challenging due to several phramcaokinetic and pharmacodynamioc limitations. Zosuquidar, is a potent and relatively selective ABCB1 inhibitor [10,16,17]. It inhibits ABCB1 mediated efflux and exhibits less activity against other transporters, including MRP1 and BCRP [17]. The clinical studies reports zosuquidar inhibit P-glycoprotein function in acute myeloid leukaemia (AML) [18]. However, the randomized the phase III clinical trial on AML patients showed limiting clinical utility [19]. The selective ABCB1 is the major concern in limiting the clinical utility of these developed agents [20,21]. Hence, the search for alternative ABCB1 modulators has explored synthetic compounds, natural products, and structure-guided medicinal chemistry. Several synthetic scaffolds, including triazolo[1,5-a]pyrimidines, 4-indolyl quinazolines, β-carbolines, coumarin-containing triazolopyrimidines, substituted benzimidazoles, and curcumin derivatives, and these studies have demonstrated ABCB1 modulating activity in preclinical investigations [22–27]. Natural products, particularly flavonoids, have also attracted attention because of their structural diversity and potential to modulate transporter activity [28,29]. Quercetin and cyanidin-3-O-sophoroside have been reported to exert synergistic inhibitory effects on ABCB1 [30]. The identification of effective modulators remains challenging because transporter recognition depends on molecular shape, physicochemical properties, ligand flexibility, and the conformational state of the binding cavity.

Computer aided drug discovery has provides a means of prioritising compounds for experimental evaluation. Pharmacophore based screening has identified potential ABCB1 inhibitors from chemical libraries [31], while database mining combined with molecular dynamics (MD) simulations has been applied to investigate potential natural-product modulators [32]. More recently, machine learning approaches integrated with MD simulations have been explored to predict and characterise interactions between ABCB1 and its ligands [33]. Shape-based screening is particularly relevant to ABCB1 because it can identify molecules with three-dimensional features resembling a known inhibitor even when their chemical scaffolds differ. Combining shape similarity with molecular fingerprints and physicochemical filters can further reduce the search space by prioritising compounds with complementary structural and property profiles.

However, conventional molecular docking against a single receptor structure may limitations in representing ABCB1 in it's stable form, because its drug binding cavity undergoes conformational changes during substrate recognition and transport. MD simulations have demonstrated that transporter dynamics are influenced by the surrounding lipid membrane and by rearrangements of the transmembrane helices [34,35]. Moreover, systematic docking across different transporter conformations has shown that predicted inhibitor compatibility can vary with the receptor state [36]. Ensemble docking addresses this limitation by evaluating ligands against multiple receptor conformations, thereby incorporating aspects of target flexibility into virtual screening [37]. In addition, the structural evidence for paired inhibitor occupancy suggests that multiple-ligand simultaneous docking (MLSD) may provide a useful complementary strategy for investigating binding arrangements that involve two ligand molecules within the ABCB1 drug-binding region [8–10].

In the present study, an integrated computational workflow was developed to identify potential ABCB1 modulators from the ZINC20 database using zosuquidar as the reference ligand. Approximately 1.5 million compounds were initially selected according to molecular weight and lipophilicity criteria centred on zosuquidar. The resulting library was screened for

3D shape similarity and FCFP4-like Morgan fingerprints, followed by physicochemical filtering based on hydrogen bond donor and acceptor counts, rotatable bonds, and topological polar surface area. The filtered compounds were subjected to MLSD against the zosuquidar binding region of human ABCB1 (PDB ID: 7A6F), using two copies of each ligand to investigate the possibility of paired occupancy. Selected compounds were subsequently evaluated by ensemble docking against 23 receptor conformations. Four high ranking candidates and zosuquidar were then investigated using 100 ns transmembrane MD simulations, followed by analyses of structural stability, residue flexibility, compactness, solvent-accessible surface area, hydrogen bonding, principal component analysis, and MM-GBSA binding free energies. By integrating shape and property guided screening, paired-ligand docking, receptor ensemble evaluation, and MD based analysis, this study aimed to prioritise computationally promising ABCB1 binding candidates for subsequent experimental validation.

1. Methods

1.1 Protein preparation

The cryo-EM structure of human ABCB1 bound to zosuquidar (PDB 7A6F, 3.50 Å) [8] was used in the study. The structure has missing residues in the segments between residues 1-31, 86-103, 631-693 and 1277-1280, and the loops 86-103 and 631-693, which were modelled and filled with Modeller 9.25 [38]. For docking input preparation, the bound inhibitor, the antibody fragment and all water molecules were deleted. The protonation states at pH 7.4 were assigned with PROPKA and polar hydrogen were kept for docking studies, and the structure was converted to PDBQT format with AutoDockTools. The grid box was centred on the zosuquidar site at x = 161.296, y = 158.600, z = 159.271 with dimensions 18 × 18 × 20 Å, which encloses the central drug binding pocket and the adjoining access tunnel.

1.2 Ligand library and ligand-based virtual screening

Compound library in SDF format was retrieved from ZINC20 [39]. An initial set of 1,593,937 compounds on the basis of molecular weight and logP values matching zosuquidar (MW 527.6 Da, logP 4.9) were retained. The virtual screening was performed with VSFlow open source command line tool [40]. The smiles (Simplified Molecular Input Line Entry System) notation of zosuquidar was used as a query. The 3D shape similarity search and the FCFP4-like Morgan fingerprints search resulted in 53,047 molecules. These were further filtered on the basis of physicochemical profile of zosuquidar using the VSFlow property filters, in the order hydrogen-bond donors, hydrogen-bond acceptors, rotatable bonds and topological polar surface area, resulting in 39,987, 25,487, 12,217 and finally 826 compounds, respectively during each filtering step. The structures of final 876 hits were interconverted and protonated for docking with Open Babel [41].

1.3 Multiple-ligand simultaneous docking

In cryo-EM structure of ABCB1 the inhibitor zosuquidar binds in pair [8,10], hence each of the 826 compounds was docked as a pair simultaneously in the grid box, using the multiple ligand simultaneous docking (MLSD) strategy [42] using AutoDock Vina (Version 1.2.6) [43] with exhaustiveness 16, energy range 5 kcal mol^{-1} and grid spacing 1 Å. The binding energies are reported as a combined binding energy of a pair. For comparative study zosuquidar was docked employing same docking conditions.

1.4 Ensemble docking and consensus ranking

The preliminary MLSD resulted in 82 hits that scored better than zosuquidar. These were re-docked against 23 ABCB1 receptor conformations. These conformations were obtained from Rotamerically Induced Perturbations with Langevin dynamics (L-RIP) method [44]. For each compound the mean, standard deviation and best score across the 23 conformations were computed, and compounds were ranked on the difference between their ensemble mean and that of zosuquidar. The twenty best-ranked compounds were analyzed for their interactions and binding energies.

1.5 Molecular dynamics simulations

Four top hits, ZINC001463799743, ZINC000256027845, ZINC001315607657 and ZINC000139632919, were subjected to molecular dynamics simulations along with the complex of ABCB1 with reference zosuquidar. The molecular dynamics simulation protocol followed as reported in our earlier work [30]. Briefly, each complex was embedded in a 1-palmitoyl-2-oleoyl-sn-glycero-3-phosphocholine (POPC) bilayer assembled in CHARMM-GUI [45], with the transporter oriented in the membrane according to the Orientations of Proteins in Membranes database [46]. Ligand topologies were generated with the CHARMM General Force Field (CGenFF) from the docked coordinates [47]. The system was solvated so that water extended roughly 10 Å beyond the protein on both sides of the bilayer, using the TIP3P water model [48], and neutralised with 150 mM KCl. MD simulations were performed with Gromacs 2020.4 [49]. Each system was first energy minimised with a steepest-descent integrator until Fmax reached 10 kJ mol^{-1}. Later, six stage equilibration was performed. The first three at a 1 fs time step and the remaining three stages at 2 fs. The first two stages were run in the NVT ensemble with a Berendsen thermostat [50], and the later NPT stages added a Berendsen barostat with semiisotropic pressure coupling at 1 bar. Protein, membrane and solvent were coupled separately, and the temperature was held at 310 K throughout the simulation. Long-range electrostatics were treated by particle mesh Ewald [51] with a 1.2 nm cut-off, and van der Waals interactions used the same 1.2 nm cut-off. All bonds were constrained with LINCS [52]. Production runs of 100 ns were carried out with a Nose-Hoover thermostat [53,54] and a Parrinello–Rahman barostat [55], with trajectories saved at every

10 ps. Trajectories were corrected for periodicity and least-squares fitted to the protein backbone before analysis. Backbone root mean square deviation (RMSD), Ligand RMSD fitting to backbone, per residue root-mean-square fluctuation (RMSF), radius of gyration (Rg) and solvent accessible surface area (SASA) were computed. Hydrogen bonds formed between ligand and the ABCB1 were calculated. Essential dynamics was performed by principal component analysis of the backbone covariance matrix, and Gibbs free energy landscapes were constructed over the first two principal components. Dynamic cross-correlation matrices were computed over the Cα atoms to describe correlated and anti-correlated domain motions.

1.6 Binding free energy

Binding free energies were estimated by the molecular mechanics generalised Born surface area method in gmx_MMPBSA 1.6.1 [56], using 25 evenly spaced frames from each trajectory at 310 K with ESURF from LCPO surface areas. As ligands in each complex were taken as a pair the reported ΔG refers to the combined binding of the ligand pair. The entropic term was obtained by the interaction entropy approximation [57] from the last seven frames, and ΔGbinding = ΔTOTAL − TΔS.

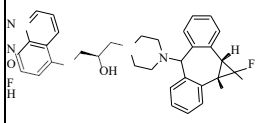
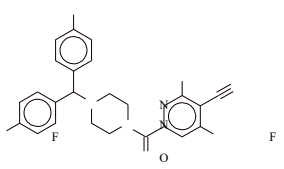
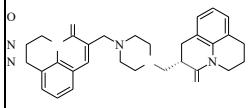
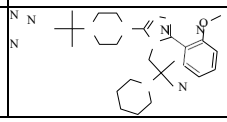
2. Results and discussion

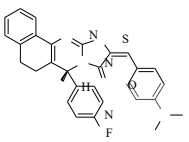
2.1 Virtual screening

The virtual screening protocol sequentially reduced 1,593,937 ZINC20 molecules to 826 docking candidates, showing a 1,930 fold enrichment (**Figure 1**). The 3D shape alignment to zosuquidar together with FCFP4-like Morgan fingerprints was found were selective filtering step, which eliminated 97% of the starting set and leaving 53,047 molecules. The subsequent property filters eliminated a further 98% giving hydrogen-bond donors reduced the set to 39,987, acceptors to 25,487, rotatable bonds to 12,217 and the polar surface area filter to 826. Shape and fingerprint similarity were applied first so that molecules were selected for resembling zosuquidar in 3D space and imitate or bind analogously at ABCB1. The physicochemical filters was set to obtain chemically relevant drug like molecules from shape analogus set. The final 4 hits obtained from virtual screening and subsequent molecular docking and ensemble docking share a Tanimoto similarities of only 0.14–0.21 with the query zosuquidar (**Table 1**). For a target ABCB1, where the drug binding and access tunnel feature compliments shape, hydrophobicity and aromatic surface than on a defined pharmacophore [5,6], and hence this virtual screening protocol was expected to offer distinct advantages than traditional virtual screening workflows.

Figure 1: Virtual screening protocol.

Table 1: Properties, similarity to zosuquidar and ensemble docking performance of the compounds taken to molecular dynamics. Similarity values from the VSFlow shape and fingerprint screen; docking values from ensemble docking over 23 receptor conformations.

Compound	Formula	Details	Values
Zosuquidar (reference)		MW (Da)	527.6
		Shape similarity	-
		3D FP similarity	-
		Tanimoto	-
		Ensemble mean (kcal mol^{-1})	−15.03 (0.75)
		Best score (kcal mol^{-1})	−16.68
ZINC00146 3799743		MW (Da)	449.4
		Shape similarity	0.466
		3D FP similarity	0.251
		Tanimoto	0.186
		Ensemble mean (kcal mol^{-1})	−17.44 (0.71)
		Best score (kcal mol^{-1})	−18.79
ZINC00025 6027845		MW (Da)	482.6
		Shape similarity	0.373
		3D FP similarity	0.169
		Tanimoto	0.210
		Ensemble mean (kcal mol^{-1})	−17.15 (0.82)
		Best score (kcal mol^{-1})	−18.73
ZINC00131 5607657		MW (Da)	457.7
		Shape similarity	0.395
		3D FP similarity	0.091
		Tanimoto	0.167

Compound	Formula	Details	Values
		Ensemble mean (kcal mol^{-1})	−16.89 (0.9)
		Best score (kcal mol^{-1})	−18.87
ZINC00013 9632919		MW (Da)	483.6
		Shape similarity	0.346
		3D FP similarity	0.268
		Tanimoto	0.143
		Ensemble mean (kcal mol^{-1})	−16.48 (1.30)
		Best score (kcal mol^{-1})	−19.28

2.2

2.3 Multi Ligand Simultaneous Docking (MLSD)

All 826 compounds were docked as ligand pairs into the drug-binding pocket and access tunnel of ABCB1 (PDB ID: 7A6F). Scores are correspondingly large, in the -12 to -19 kcal mol^{-1} range, because they included scores for a pair. Eighty two compounds showed binding free energy better than zosuquidar (−15.0249 kcal mol^{-1}). These hits were subjected to the ensemble docking.

2.4 Ensemble docking for 23 unique conformations of ABCB1

The LRIP based MD simulation of apo ABCB1 resulted in 23 unique conformations, each differing in the dynamic state of drug binding cavity and adjacent access tunnel. Eight two hits which outperform in MLSD preliminary docking studies were docked against all 23 conformations. The binding free energies against all 23 conformations for all 82 hits were further analyzed and compared to binding free energy of reference zosuquidar. From the mean binding free energy for respective hit and mean

binding free energy of zosuquidar, the hits were further selected on the basis of ScoreX, which was calculated using the equation.

$ScoreX = BE_{ZQU} - BE_{Hit\ (i)}$

Where, BEZQU is the mean docking score of zosuquidar across 23 receptor conformations and BEHit(i) is the corresponding mean for hit (i). The ScoreX are given in **Table 2**.

Table 2: Top 20 hits identification

Compound	Score X	Compound	Score X
Zosuquidar	**0**	ZINC000027907116	1.420
ZINC001463799743	2.415	ZINC000070687149	1.359
ZINC000256027845	2.122	ZINC000048345511	1.345
ZINC000225862568	1.962	ZINC001164946192	1.333
ZINC001165001099	1.931	ZINC000248093156	1.303
ZINC000225862585	1.924	ZINC000022236410	1.297
ZINC001315607657	1.871	ZINC001164912772	1.247
ZINC000070673140	1.814	ZINC000085902231	1.230
ZINC000139632919	1.594	ZINC001164883877	1.156
ZINC000096316576	1.523	ZINC000225366988	1.141
ZINC000070673141	1.428		

The visual inspection of the interactions pair of ligand of zosuquidar and respective hit was evaluated. The top four hits the interactions were almost similar to those of interactions formed by zosuquidar (**Figure 2**). Zosuquidar formed hydrogen bonds to Gln990 and Glu875 and formed stacking and alkyl interactions with Trp232, Phe303, Leu65, Leu339, Ala233, Met876, Met949, Met986, Ala987, Tyr950 and Val991 (**Table 3**). Each of the top ten hits reproduced almost all the π-π stacking and T-shaped interactions with the tunnel aromatics Phe272, Phe312, Phe952, Tyr922 and Trp201, one or two hydrogen bonds to a glutamine-glutamate pair (Gln959 with Glu844, an sometimes with Gln694 or Gln164 with Ser165 and Ser313), and a broad hydrophobic interactions with Ile268, Ile275, Ile309, Leu34, Leu205, Leu308, Leu848, Ala198, Ala202, Ala271, Ala956, Met38, Met845, Met918 and Val960. The access tunnel which is phenylalanine-rich channel mostly forms a π-stacking interactions and hence there might be fewer polar interactions [8]. Two of the hits, ZINC000070673140 and ZINC000139632919, formed no hydrogen bond but have better binding energy due to such hydrophobic interactions. The binding energy against a single conformation of ABCB1 has a limitation of conformational rigidity, where as a wide conformational range offer structural flexibility and is a better approach than the conventional docking [58]. The 82 compounds having better binding energies than zosuquidar in the initial docking were therefore re-docked against 23 receptor conformations and ranked on their ensemble ScoreX (**Figure 3**).

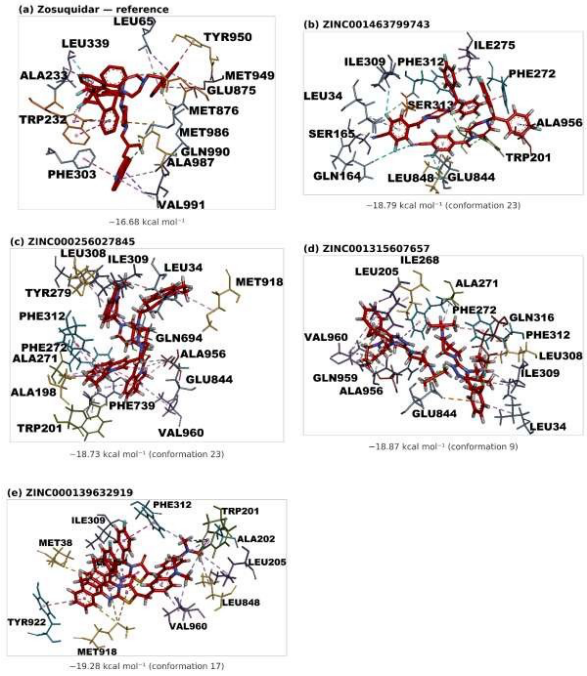


Figure 2: Docked binding modes in the zosuquidar site of ABCB1 for (a) zosuquidar and (b-e) the four respective hits.

Table 3. Interactions of zosuquidar and the top 10 hits at the binding sites of ABCB1.

Compound	Binding energy (kcal mol^{-1})	Hydrogen bonds	Other key interactions
Zosuquidar	−16.68	Gln990, Glu875	Trp232, Phe303 (π–π and T-shaped); Leu65, Leu339, Ala233, Met876, Met949, Met986, Ala987, Tyr950, Val991
ZINC001463799743	−18.79	Gln164, Ser165, Ser313, Glu844	Phe272, Phe312, Trp201; Ile275, Ile309, Leu34, Leu848, Ala956
ZINC000256027845	−18.73	Gln694, Glu844	Phe272, Phe312, Phe739, Trp201, Tyr279; Ala271, Val960, Met918, Leu308, Ile309, Leu34, Ala956
ZINC000225862568	−18.54	Gln959, Glu844	Phe952, Trp201; Ile275, Ile309, Ala198, Ala202, Leu34, Leu848, Met845
ZINC001165001099	−15.87	Gln990, Ser341	Phe728, Phe983, Phe336; Ile306, Ile340, Met69
ZINC000225862585	−18.62	Gln959, Gln694	Phe697, Tyr276, Phe272, Trp201, Phe312, Phe952; Ile275, Leu308, Ile309, Ala956, Met955, Met845, Met38
ZINC001315607657	−18.87	Gln316, Gln959, Glu844	Phe272, Phe312; Leu205, Ile268, Ala271, Leu308, Ile309, Leu34, Val960, Ala956
ZINC000070673140	−18.47	none observed	Phe952, Tyr276, Phe963, Trp201; Leu308, Ala956, Leu693, Met845
ZINC000096316576	−17.81	Gln959, Glu844	Phe312, Trp201; Ile275, Ile268, Leu34, Ala198, Leu308, Ile309, Ala202, Ala271
ZINC000139632919	−19.28	none observed	Phe312, Trp201, Tyr922; Ile309, Leu205, Leu848, Val960, Ala202, Met38, Met918
ZINC000070673141	−17.12	Gln959, Glu844	Phe272, Trp201; Ile268, Ile275, Met38,

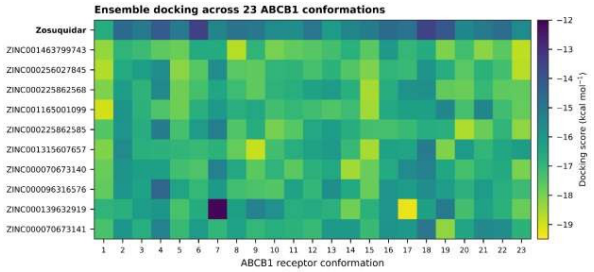


Figure 3: Ensemble docking scores of zosuquidar and the ten best-ranked hits across 23 ABCB1 receptor conformations.

Zosuquidar averaged -15.03 ± 0.75 kcal mol^{-1} across the ensemble, with a best score of -16.68 kcal mol^{-1}. The ten best-ranked hits all averaged between -16.45 and -17.44 kcal mol^{-1}. ZINC001463799743 led the ranking at -17.44 ± 0.71 kcal mol^{-1} and, importantly, has the best scoreX than zosuquidar, on all 23 conformations. Similarly, ZINC000256027845, ZINC000225862568, ZINC001165001099, ZINC000225862585, ZINC001315607657 and ZINC000070673140 were likewise better than zosuquidar in every conformation tested. Specifically, the hit ZINC000139632919 produced the single best score in the entire study,

−19.282 kcal mol^{-1} against conformation 17. However, on other conformations its binding energy is higher. Hence, taking a mean of binding energy assisted in further selecting the top hits.

2.5 Hit selection for membrane simulations

Four compounds spanning the top of the ranking were subjected to molecular dynamics alongside zosuquidar (**Table 1**). These hits are chemically diverse, a rigid tetrafluorinated aromatic (ZINC001463799743), a flexible diaryl species with four basic nitrogens (ZINC000256027845), a highly aliphatic polyamine (ZINC001315607657) and a thioether-containing fluoroaromatic (ZINC000139632919). All four fall within 30–80 Da of zosuquidar's molecular weight, consistent with the shape-matching step, while differing substantially in polarity and flexibility.

2.6 RMSD evaluations for backbone stability

Every complex reached a stable RMSD plateau and remained stable (**Figure 4a**). Backbone RMSD rose over the first 10–20 ns and then fluctuated about a constant value for the remaining 80 ns, with 100 ns averages between 0.359 and 0.502 nm (**Table 4**). For a ABCB1 with significantly large number of residues (1,245 residues) consisting of two mobile nucleotide-binding domains, these RMSD deviations are modest and indicate that the folding was preserved in all five systems. The ZINC001463799743 complex was the most rigid and most stable, averaging 0.359 ± 0.054 nm, appreciably below the zosuquidar reference at 0.502 ±

0.052 nm. ZINC000256027845 (0.409 ± 0.037 nm) was also reasonably stable than the reference, and its standard deviation was the smallest of the set, meaning it not only deviated less but deviated less. ZINC001315607657 (0.465 ± 0.072 nm) and ZINC000139632919 (0.476 ± 0.041 nm) showed modest deviations but slightly higher than the zosuquidar.

Figure 4: Backbone RMSD of ABCB1 (a) and of the ligand at central drug-binding pocket (b).

Table 4. Trajectory averages over 100 ns; standard deviations in parentheses. Ligand RMSD is reported separately for the copy in the central drug-binding pocket and the copy in the access tunnel.

Parameter	Zosuquidar	ZINC001463799743	ZINC000256027845	ZINC001315607657	ZINC000139632919
Backbone RMSD (nm)	0.502 (0.052)	0.359 (0.054)	0.409 (0.037)	0.465 (0.072)	0.476 (0.041)
Ligand RMSD, central pocket (nm)	0.191 (0.039)	0.168 (0.019)	0.287 (0.045)	0.740 (0.102)	0.489 (0.047)

Parameter	Zosuquidar	ZINC001463799743	ZINC000256027845	ZINC001315607657	ZINC000139632919
Ligand RMSD, access (nm)	0.250 (0.047)	0.337 (0.042)	0.526 (0.063)	8.383 (3.480)	0.277 (0.038)
RMSF (nm)	0.183 (0.108)	0.207 (0.081)	0.183 (0.076)	0.246 (0.136)	0.187 (0.082)
Radius gyration (nm)	3.971 (0.016)	4.045 (0.025)	4.017 (0.021)	4.027 (0.027)	3.980 (0.022)
SASA (nm2)	551.92 (9.50)	560.39 (7.81)	541.69 (11.43)	567.36 (13.14)	552.64 (13.43)

2.7 Ligand RMSD relative to ABCB1 backbone atoms

Since every complex has two ligands as a pair, the RMSD was evaluated separately at each site **(Figure 5**). The ligands at the central drug-binding pocket (site 1) stayed bound in all five systems, with RMSD averages from 0.168 to 0.740 nm. ZINC001463799743 remained most stable with an average RMSD of 0.168 ± 0.019 nm, better than zosuquidar with an average of

0.191 ± 0.039 nm. After around 40 ns, ZINC000256027845 also stabilized with an average of 0.287 ± 0.045 nm. At site 2, the access tunnel, zosuquidar showed RMSD of 0.250 ± 0.047 nm), ZINC000139632919 (0.277 ± 0.038 nm) and ZINC001463799743 (0.337 ± 0.042 nm)

and remained stable throughout the simulation period. ZINC000256027845 remained stable with slightly higher average RMSD of 0.526 ± 0.063 nm. However, ZINC001315607657, might have moved out of access tunnel and displayed no stability with an average RMSD of 8.383 ± 3.480 nm. Based on these ligand RMSD results though ZINC001315607657 showed better docking base binding free energy, may be the weaker in binding ABCB1.

Figure 5: RMSD of ligand pairs at central drug-binding pocket (site 1) (a) and access tunnel (site 2) (b).

2.8 RMSF evaluations

RMSF profiles were closely similar across all five complexes (**Figure 6**), averaging 0.183-0.246 nm. The transmembrane helices of TMD1 (residues 51-357) and TMD2 (711-1000), which form the drug binding cavity, retained rigidity with RMSF of around 0.15–0.20 nm in every system. This suggests ligand binding do not destabilize the translocation pathway. The nucleotide binding domains and the loops connecting the two halves of the transporter showed the higher RMSF and the flexibility. The zosuquidar complex with ABCB1 showed its single largest fluctuation at residue 677 (1.113 nm), in the linker region between NBD1 and TMD2, whereas the hit complexes peaked at 0.711–0.761 nm in the same region, suggesting the hits do not affect much the inter domain linker than the reference. ZINC001315607657, meanwhile, was the most flexible system overall (0.246 ± 0.136 nm) with a sharp 1.320 nm peak at residue 60 and elevated fluctuation throughout NBD1, which is consistent with the higher ligand RMSD at site 2, the access tunnel. ZINC000256027845 (0.183 ± 0.076 nm) and ZINC000139632919 (0.187 ± 0.082 nm) showed stable and lower RMSF than thee zosuquidar reference (0.183 ± 0.108 nm).

Figure 6: Per-residue RMSF. Shaded regions indicate TMD1, NBD1, TMD2 and NBD2.

2.9 Radius of gyration and solvent accessible surface area evaluations

All the complexes remained stable throughout the simulation period without loss of their compactness and no evident folding (**Figure 7a**). The Rg values range between 3.971 and 4.045 nm, with per system standard deviations of around 0.016-0.027 nm. The zosuquidar complex was the most compact with an average Rg of 3.971 ± 0.016 nm and ZINC001463799743 was comparably compact with average Rg of 4.045 ± 0.025 nm. In the case of solvent accessible surface areas (SASA) analysis showed similar and corroborating results (**Figure 7b**), where

the SASA ranged from 541.69 ± 11.43 nm^2 for ZINC000256027845 to 567.36 ± 13.14 nm^2 for ZINC001315607657, around the zosuquidar value of 551.92 ± 9.50 nm^2. ZINC000256027845 presented the smallest solvent exposed surface by around 10 nm^2 relative to the reference, indicating a stable systems.

Figure 7: Radius of gyration (a) and solvent accessible surface area of the complex (b) over 100 ns.

2.10 Hydrogen bonding

The results of hydrogen bond analysis are presented in **Figure 8** and **Table 5**. ZINC000256027845 formed the most persistent network of h-bonds averaging 1.65 ± 0.96 bonds between its two ligand copies and the protein, present in 87.1% of frames and reaching five simultaneous bonds; and as pair averaged 1.46 bonds and was engaged for 82.6% of the trajectory. This is better than the zosuquidar reference, which averaged 1.26 ± 0.49 bonds with 99.2% occupancy. ZINC001463799743 showed 0.96 ± 0.27 bonds with 94.2% occupancy, with the pair with 0.94 bonds and 94.0% occupancy. ZINC000139632919 showed slightly weaker hydrogen bonding with average 0.48 ± 0.54 H-bonds and 45.8% occupancy, with no hydrogen bonds observed in its best docked pose. Its binding is dominated by hydrophobic and aromatic interactions. ZINC001315607657 h-bonds averaged 1.06 ± 1.03 with 62.4% occupancy.

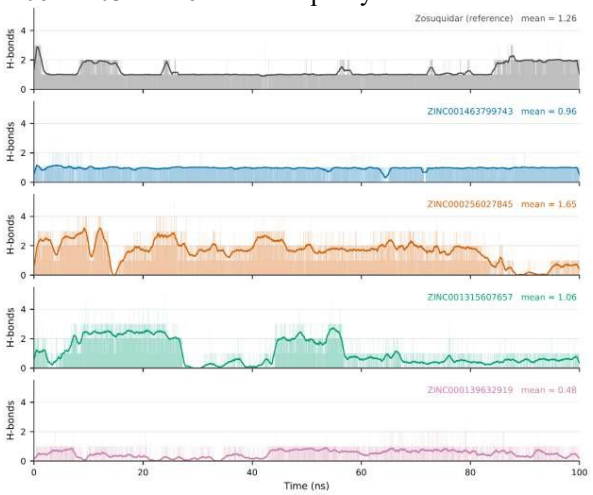


Figure 8: Hydrogen bonds between the respective ligand pairs and ABCB1 over 100 ns.

Table 5. Hydrogen bonding between ligand and the occupancy analysis

System	Site 1 mean (max)	Site 1 occupancy	Site 2 mean (max)	Site 2 occupancy	As pair mean (max)	Pair occupancy
Zosuquidar	0.99 (2)	99.0%	0.27 (3)	25.3%	1.26 (4)	99.2%
ZINC001463799743	0.02 (2)	1.9%	0.94 (2)	94.0%	0.96 (3)	94.2%
ZINC000256027845	0.19 (2)	18.6%	1.46 (4)	82.6%	1.65 (5)	87.1%
ZINC001315607657	0.69 (3)	38.3%	0.37 (3)	34.8%	1.06 (5)	62.4%
ZINC000139632919	0.43 (1)	42.5%	0.06 (2)	5.6%	0.48 (3)	45.8%

2.11 MM-GBSA calculations

Twenty five trajectory frames corresponding to the lowest energy basins from PCA essential dynamics analysis were extracted and used for the MM-GBSA calculations. Hence, the free energies obtained from MM-GBSA refer to the dominant conformational state of each complex rather than to an average over unrelated and diverse states over the MD simulation trajectories. ZINC000256027845 showed better binding affinity than zosuquidar, with ΔGbinding of -
116.93 ± 7.57, against -107.89 ± 3.41 kcal mol^{-1} for the zosuquidar (**Table 6, Figure 9**).
ZINC001315607657 (-94.72 ± 3.78) and ZINC000139632919 (-93.99 ± 3.51) showed modest ΔGbinding, while ZINC001463799743 showed poor ΔGbinding of -85.55 ± 3.97 kcal mol^{-1}. The MM-GBSA calculations showed that binding is predominately affected by van der Waals contact. ΔVDWAALS ranged from -88.51 to -119.70 kcal mol^{-1} while electrostatics contributions ranged only between from -2 to -7 kcal mol^{-1}, and the non-polar solvation energies ranged from -11 to -15 kcal mol^{-1}. The results are consistent with previous reports which suggest the hydrophobic interaction energies are important in binding affinities, where phenylalanines, leucines, isoleucines and methionines residues majorly contribute in such interactions [5,6,8]. ZINC000256027845 has the most favorable van der Waals interactions (-119.70 ± 6.69 kcal mol^{-1}, compared to -109.58 ± 3.24 for zosuquidar). The flexible diaryl part in its structure might have resulted in this favorable interaction compared to the rigid tetracyclic core of zosuquidar, which is also consistent with the SASA analysis and extensively hydrogen bonds for this hit.
In the case of ZINC001315607657 showed ΔEEL of +41.77 kcal mol^{-1} due to the presence of six nitrogen atoms in a largely aliphatic framework, the compound is protonated at physiological pH. Hence, its ΔGbinding is less favorable.

Table 6. Results of MM-GBSA calculations energy components in kcal mol^{-1}

Component	Zosuquidar	ZINC001463799743	ZINC000256027845	ZINC001315607657	ZINC000139632919
ΔVDWAALS	−109.58 (3.24)	−88.51 (3.78)	−119.70 (6.69)	−98.97 (3.53)	−97.37 (3.44)
ΔEEL	−6.67 (0.70)	−6.30 (1.02)	−5.60 (1.15)	+41.77 (1.74)	−5.67 (1.08)
ΔEGB	+17.57 (0.59)	+14.58 (1.21)	+16.34 (1.17)	−32.32 (1.75)	+16.89 (0.77)
ΔESURF	−14.05 (0.30)	−12.70 (0.51)	−14.57 (0.63)	−12.67 (0.53)	−11.78 (0.21)

Component	Zosuquidar	ZINC001463799743	ZINC000256027845	ZINC001315607657	ZINC000139632919
ΔGGAS	−116.25 (3.44)	−94.81 (3.92)	−125.31 (6.98)	−57.19 (4.80)	−103.03 (3.66)
ΔGSOLV	+3.51 (0.46)	+1.87 (1.11)	+1.77 (0.73)	−44.99 (1.47)	+5.11 (0.81)
ΔTOTAL	−112.74 (3.33)	−92.94 (3.97)	−123.54 (6.76)	−102.18 (3.78)	−97.92 (3.47)
Entropy (-TΔS)	+3.44 (0.74)	+3.92 (0.05)	+6.98 (3.41)	+4.80 (0.05)	+3.66 (0.56)
ΔGbinding	−107.89 (3.41)	−85.55 (3.97)	−116.93 (7.57)	−94.72 (3.78)	−93.99 (3.51)

ΔVDWAALS: van der Waals energy; ΔEEL: Electrostatic energies; ΔEGB: Polar solvation energy; ΔESURF: Nonpolar solvation energy; ΔGGAS = ΔVDWAALS+ΔEEL; ΔGSOLV = ΔEGB+ ΔESURF; ΔTOTAL = ΔGSOLV +ΔGGAS; ΔG binding = ΔTOTAL – TΔS (Standard
deviations are given in parentheses)

Figure 9: MM-GBSA energy components (a) and

binding free energies with standard deviations (b).

2.12 Essential dynamics, Gibb's FEL, and DCCM analysis

Principal component analysis of the backbone covariance matrix, projected onto the first two principal components as a Gibbs free energy landscape, gave almost similar results for all five complexes. Each landscape showed a small number of adjacent low energy basins rather than a broad and dispersed, multiple basins, indicating that the complexes sampled a restricted set of related conformations over 100 ns (**Figure 10**).

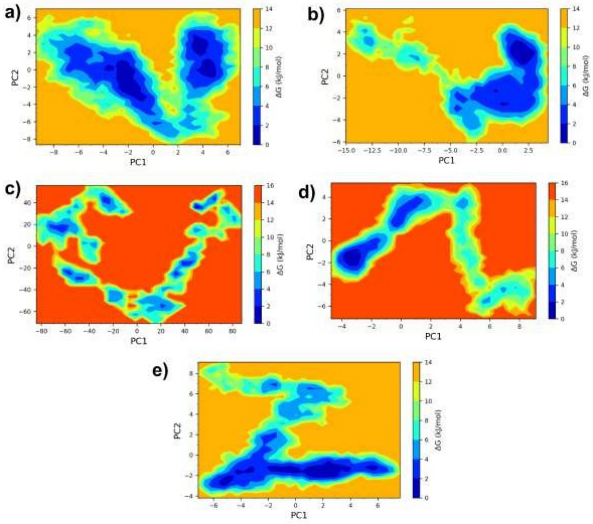


Figure 10: Gibb's FEL analysis

Dynamic cross-correlation matrices over the Cα atoms showed the correlation pattern expected for an ABC transporter, where a strong positive correlation within each transmembrane domain and within each nucleotide binding domain, and anti-correlated motion between the two halves of the molecule, indicating the scissoring of the NBDs relative to the TMDs. All the hit complexes showed a rigid, motion free state and might have occupied the drug binding cavity as well as access tunnel effectively to hold the motion of the ABCB1 intact (**Figure 11**).

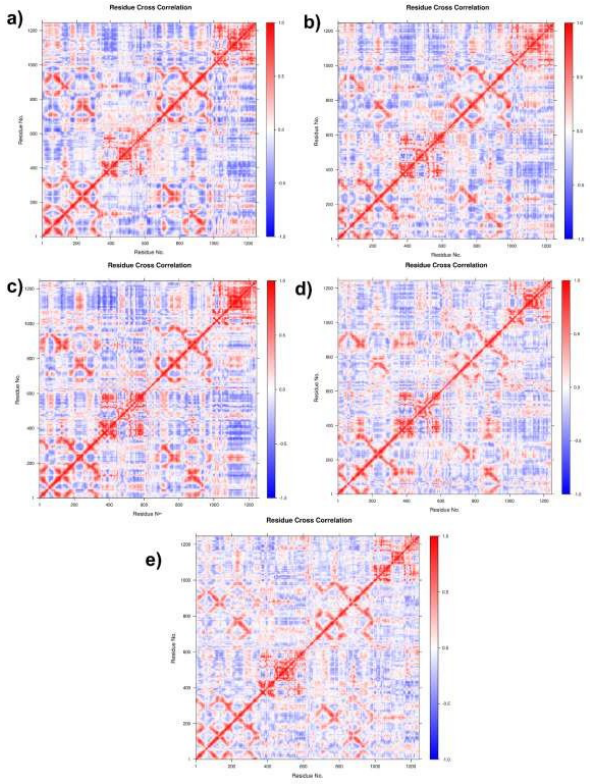


Figure 11. DCCM analysis

3. Conclusion

A shape and property guided screen of ZINC20 database against zosuquidar, followed by paired ligand docking into the zosuquidar site of human ABCB1, ensemble re-ranking across 23 receptor conformations and 100 ns molecular dynamics, identified two compounds ZINC000256027845 and ZINC001463799743. ZINC000256027845 is the stronger candidate on binding energetics which showed most favorable MM-GBSA binding free energy in the study (-116.93 ± 7.57 kcal mol^{-1}, against -107.89 ± 3.41 for zosuquidar), and ZINC001463799743 is the another hit based on other computational criteria's, with ensemble docking ranking at -17.44 ± 0.71 kcal mol^{-1} and backbone RMSD 0.359 ± 0.054 nm. The hit ZINC000139632919 is also a promising candidate with a MD simulation parameters, with better hydrophobic interactions. MD simulations studies suggested poor performance ZINC001315607657, over various MD parameters, though this hit showed good binding energy in ensemble docking. The hits ZINC000256027845, ZINC001463799743, and ZINC000256027845 could be taken further for experimental validations and for further optimization for the development of promising ABCB1 inhibitor.

References

[1] Bray F, Laversanne M, Sung H, et al. Global cancer statistics 2022: GLOBOCAN estimates of incidence and mortality worldwide for 36 cancers in 185 countries. CA A Cancer J Clinicians 2024;74:229–63. https://doi.org/10.3322/caac.21834.

[2] Sun D, Bo L, Jiang C, et al. Beyond the boundary: The emerging roles of ATP-binding

cassette transporters in multidrug resistance (MDR) and therapeutic targeting in cancer. Drug Resistance Updates 2026;84:101310. https://doi.org/10.1016/j.drup.2025.101310.

[3] Vasconcelos FC, De Souza PS, Hancio T, et al. Update on drug transporter proteins in acute myeloid leukemia: Pathological implication and clinical setting. Critical Reviews in Oncology/Hematology 2021;160:103281. https://doi.org/10.1016/j.critrevonc.2021.103281.

[4] Nicolae AC, Sîrbu CA, Dumitrescu I-B, et al. Breaking the Efflux Barrier: P-Glycoprotein and Emerging Strategies to Overcome Multidrug Resistance in Cancer. Cancers 2026;18:2047. https://doi.org/10.3390/cancers18132047.

[5] Molecular Basis of the Polyspecificity of P-Glycoprotein (ABCB1). ABC Transporters and Cancer, vol. 125, Elsevier; 2015, p. 71–96. https://doi.org/10.1016/bs.acr.2014.10.003.

[6] Xia D, Zhou F, Esser L. Emerging consensus on the mechanism of polyspecific substrate recognition by the multidrug transporter P-glycoprotein. CDR 2019. https://doi.org/10.20517/cdr.2019.22.

[7] Le CA, Harvey DS, Aller SG. Structural definition of polyspecific compensatory ligand recognition by P-glycoprotein. IUCrJ 2020;7:663–72. https://doi.org/10.1107/S2052252520005709.

[8] Nosol K, Romane K, Irobalieva RN, et al. Cryo-EM structures reveal distinct mechanisms of inhibition of the human multidrug transporter ABCB1. Proc Natl Acad Sci USA 2020;117:26245–53. https://doi.org/10.1073/pnas.2010264117.

[9] Loo TW, Bartlett MC, Clarke DM. Simultaneous Binding of Two Different Drugs in the Binding Pocket of the Human Multidrug Resistance P-glycoprotein. Journal of Biological Chemistry 2003;278:39706–10. https://doi.org/10.1074/jbc.M308559200.

[10] Alam A, Küng R, Kowal J, et al. Structure of a zosuquidar and UIC2-bound human-mouse chimeric ABCB1. Proc Natl Acad Sci USA 2018;115. https://doi.org/10.1073/pnas.1717044115.

[11] Moosavi F, Hassani B, Mortazavi M, et al. Protein Kinase Inhibitors as Regulators of ABC Transporters in Overcoming Cancer Multidrug Resistance: A Comprehensive Review of Recent Advances. Cancers 2026;18:1957. https://doi.org/10.3390/cancers18121957.

[12] Fracasso PM, Fisher GA, Goodner SA, et al. A Phase I Trial of the ABCB1 Inhibitor, Oral Valspodar, in Combination With Paclitaxel in Patients With Advanced Solid Tumors. American Journal of Clinical Oncology 2023;46:353–9. https://doi.org/10.1097/COC.0000000000001014.

[13] Lacayo NJ, Duran GE, Sikic BI. Modulation of resistance to idarubicin by the cyclosporin PSC 833 (valspodar) in multidrug-resistant cells. J Exp Therapeutics 2003;3:127–35. https://doi.org/10.1046/j.1359-4117.2003.01088.x.

[14] Loo TW, Clarke DM. Tariquidar inhibits P-glycoprotein drug efflux but activates ATPase activity by blocking transition to an open conformation. Biochemical Pharmacology 2014;92:558–66. https://doi.org/10.1016/j.bcp.2014.10.006.

[15] Chen H, Shien K, Suzawa K, et al. Elacridar, a third-generation ABCB1 inhibitor, overcomes resistance to docetaxel in non-small cell lung cancer. Oncology Letters 2017;14:4349–54. https://doi.org/10.3892/ol.2017.6678.

[16] Dantzig A, Law K, Cao J, et al. Reversal of Multidrug Resistance by the P-Glycoprotein Modulator, LY335979, from the Bench to the Clinic. CMC 2001;8:39–50. https://doi.org/10.2174/0929867013373903.

[17] Shepard RL, Cao J, Starling JJ, et al. Modulation of P-glycoprotein but not MRP1- or BCRP-mediated drug resistance by LY335979. Intl Journal of Cancer 2003;103:121–5. https://doi.org/10.1002/ijc.10792.

[18] Gerrard G, Payne E, Baker RJ, et al. Clinical effects and P-glycoprotein inhibition in patients with acute myeloid leukemia treated with zosuquidar trihydrochloride, daunorubicin and cytarabine. Haematologica 2004;89:782–90.

[19] Cripe LD, Uno H, Paietta EM, et al. Zosuquidar, a novel modulator of P-glycoprotein, does not improve the outcome of older patients with newly diagnosed acute myeloid leukemia: a randomized, placebo-controlled trial of the Eastern Cooperative Oncology Group 3999. Blood 2010;116:4077–85. https://doi.org/10.1182/blood-2010-04-277269.

[20] Marcelletti JF, Sikic BI, Cripe LD, et al. Evidence of a role for functional heterogeneity in multidrug resistance transporters in clinical trials of P-glycoprotein modulation in acute myeloid leukemia. Cytometry Part B Clinical 2019;96:57–66. https://doi.org/10.1002/cyto.b.21737.

[21] Marcelletti JF, Multani PS, Lancet JE, et al. Leukemic blast and natural killer cell P-glycoprotein function and inhibition in a clinical trial of zosuquidar infusion in acute myeloid leukemia. Leukemia Research 2009;33:769–74. https://doi.org/10.1016/j.leukres.2008.09.020.

[22] Wang S, Wang S-Q, Teng Q-X, et al. Discovery of the Triazolo[1,5- *a*]Pyrimidine-Based Derivative WS-898 as a Highly Efficacious and Orally Bioavailable ABCB1 Inhibitor Capable of Overcoming Multidrug Resistance. J Med Chem 2021;64:16187–204. https://doi.org/10.1021/acs.jmedchem.1c01498.

[23] Yuan S, Wang B, Dai Q-Q, et al. Discovery of New 4-Indolyl Quinazoline Derivatives as Highly Potent and Orally Bioavailable P-Glycoprotein Inhibitors. J Med Chem 2021;64:14895–911. https://doi.org/10.1021/acs.jmedchem.1c01452.

[24] Wang Y, Ding N, Zhao Y, et al. Design, synthesis, and biological evaluation of β-carboline derivatives as ABCB1 inhibitors for reversing multidrug resistance. European Journal of

[25] Hmone NY, Tian X, Zhou D, et al. Discovery of novel coumarin-containing triazolo[1,5-a]pyrimidine derivatives as potent ABCB1 inhibitor for modulation of multidrug resistance. Journal of Enzyme Inhibition and Medicinal Chemistry 2026;41:2629074. https://doi.org/10.1080/14756366.2026.2629074.

[26] Abdelhafiz AHA, Serya RAT, Lasheen DS, et al. Molecular design, synthesis and biological evaluation of novel 1,2,5-trisubstituted benzimidazole derivatives as cytotoxic agents endowed with ABCB1 inhibitory action to overcome multidrug resistance in cancer cells. Journal of Enzyme Inhibition and Medicinal Chemistry 2022;37:2710–24. https://doi.org/10.1080/14756366.2022.2127700.

[27] Sagnou M, Novikov FN, Ivanova ES, et al. Novel curcumin derivatives as P-glycoprotein inhibitors: Molecular modeling, synthesis and sensitization of multidrug resistant cells to doxorubicin. European Journal of Medicinal Chemistry 2020;198:112331. https://doi.org/10.1016/j.ejmech.2020.112331.

[28] Kumar A, Jaitak V. Natural products as multidrug resistance modulators in cancer. European Journal of Medicinal Chemistry 2019;176:268–91. https://doi.org/10.1016/j.ejmech.2019.05.027.

[29] Cui J, Liu X, Chow LMC. Flavonoids as P-gp Inhibitors: A Systematic Review of SARs. CMC 2019;26:4799–831. https://doi.org/10.2174/0929867325666181001115225.

[30] Singh K, Patil RB, Patel V, et al. Synergistic Inhibitory Effect of Quercetin and Cyanidin-3O-Sophoroside on ABCB1. IJMS 2023;24:11341. https://doi.org/10.3390/ijms241411341.

[31] Zhang S, Wei Y, Li Q, et al. Pharmacophore-Based Drug Design and Biological Evaluation of Novel ABCB1 Inhibitors. Chem Biol Drug Des 2013;81:349–58. https://doi.org/10.1111/cbdd.12081.

[32] Ibrahim MAA, Abdeljawaad KAA, Abdelrahman AHM, et al. SuperNatural inhibitors to reverse multidrug resistance emerged by ABCB1 transporter: Database mining, lipid-mediated molecular dynamics, and pharmacokinetics study. PLoS ONE 2023;18:e0288919. https://doi.org/10.1371/journal.pone.0288919.

[33] Su J, Wu Y, Xiong W, et al. Integrated machine learning and molecular dynamics framework for predicting and elucidating ABCB1 allocrite interactions. Briefings in Bioinformatics 2026;27:bbag106. https://doi.org/10.1093/bib/bbag106.

[34] Domicevica L, Koldsø H, Biggin PC. Multiscale molecular dynamics simulations of lipid interactions with P-glycoprotein in a complex membrane. Journal of Molecular Graphics and Modelling 2018;80:147–56. https://doi.org/10.1016/j.jmgm.2017.12.022.

[35] Mora Lagares L, Pérez-Castillo Y, Minovski N, et al. Structure–Function Relationships in the Human P-Glycoprotein (ABCB1): Insights from Molecular Dynamics Simulations. IJMS 2021;23:362. https://doi.org/10.3390/ijms23010362.

[36] Elbahnsi A, Dragomirescu CD, Palumbo N, et al. Mapping the inhibition landscape of P-glycoprotein via conformational ensemble docking. Sci Rep 2026;16:15393. https://doi.org/10.1038/s41598-026-46760-y.

[37] Sørensen J, Demir Ö, Swift RV, et al. Molecular Docking to Flexible Targets. In: Kukol A, editor. Molecular Modeling of Proteins, vol. 1215, New York, NY: Springer New York; 2015, p. 445–69. https://doi.org/10.1007/978-1-4939-1465-4_20.

[38] Webb B, Sali A. Comparative Protein Structure Modeling Using MODELLER. CP in Bioinformatics 2016;54. https://doi.org/10.1002/cpbi.3.

[39] Irwin JJ, Tang KG, Young J, et al. ZINC20─A Free Ultralarge-Scale Chemical Database for Ligand Discovery. Journal of Chemical Information and Modeling 2020;60:6065–73. https://doi.org/10.1021/acs.jcim.0c00675.

[40] Jung S, Vatheuer H, Czodrowski P. VSFlow: an open-source ligand-based virtual screening tool. J Cheminform 2023;15:40. https://doi.org/10.1186/s13321-023-00703-1.

[41] O'Boyle NM, Banck M, James CA, et al. Open Babel: An open chemical toolbox. J Cheminform 2011;3:33. https://doi.org/10.1186/1758-2946-3-33.

[42] Li H, Li C. Multiple ligand simultaneous docking: Orchestrated dancing of ligands in binding sites of protein. J Comput Chem 2010;31:2014–22. https://doi.org/10.1002/jcc.21486.

[43] Trott O, Olson AJ. AutoDock Vina: Improving the speed and accuracy of docking with a new scoring function, efficient optimization, and multithreading. J Comput Chem 2010;31:455–61. https://doi.org/10.1002/jcc.21334.

[44] Kokh DB, Czodrowski P, Rippmann F, et al. Perturbation Approaches for Exploring Protein BindingSite Flexibility to Predict Transient Binding Pockets. Journal of Chemical Theory and Computation 2016;12:4100–13. https://doi.org/10.1021/acs.jctc.6b00101.

[45] Jo S, Kim T, Iyer VG, et al. CHARMM-GUI: A web-based graphical user interface for CHARMM. J Comput Chem 2008;29:1859–65. https://doi.org/10.1002/jcc.20945.

[46] Lomize MA, Pogozheva ID, Joo H, et al. OPM database and PPM web server: resources for positioning of proteins in membranes. Nucleic Acids Research 2012;40:D370–6. https://doi.org/10.1093/nar/gkr703.

[47] Vanommeslaeghe K, Hatcher E, Acharya C, et al. CHARMM general force field: A force field for drug-like molecules compatible with the CHARMM

all-atom additive biological force fields. J Comput Chem 2010;31:671–90. https://doi.org/10.1002/jcc.21367.

[48] Jorgensen WL, Chandrasekhar J, Madura JD, et al. Comparison of simple potential functions for simulating liquid water. The Journal of Chemical Physics 1983;79:926–35. https://doi.org/10.1063/1.445869.

[49] Abraham MJ, Murtola T, Schulz R, et al. GROMACS: High performance molecular simulations through multi-level parallelism from laptops to supercomputers. SoftwareX 2015;1–2:19–25. https://doi.org/10.1016/j.softx.2015.06.001.

[50] Berendsen HJC, Postma JPM, Van Gunsteren WF, et al. Molecular dynamics with coupling to an external bath. The Journal of Chemical Physics 1984;81:3684–90. https://doi.org/10.1063/1.448118.

[51] Darden T, York D, Pedersen L. Particle mesh Ewald: An $N \cdot \log(N)$ method for Ewald sums in large systems. The Journal of Chemical Physics 1993;98:10089–92. https://doi.org/10.1063/1.464397.

[52] Hess B, Bekker H, Berendsen HJC, et al. LINCS: A linear constraint solver for molecular simulations. J Comput Chem 1997;18:1463–72. https://doi.org/10.1002/(SICI)1096-987X(199709)18:12%3C1463::AID-JCC4%3E3.0.CO;2-H.

[53] Nosé S. A unified formulation of the constant temperature molecular dynamics methods. The Journal of Chemical Physics 1984;81:511–9. https://doi.org/10.1063/1.447334.

[54] Hoover WG. Canonical dynamics: Equilibrium phase-space distributions. Phys Rev A 1985;31:1695–7. https://doi.org/10.1103/PhysRevA.31.1695.

[55] Parrinello M, Rahman A. Polymorphic transitions in single crystals: A new molecular dynamics method. Journal of Applied Physics 1981;52:7182–90. https://doi.org/10.1063/1.328693.

[56] Valdés-Tresanco MS, Valdés-Tresanco ME, Valiente PA, et al. gmx_MMPBSA: A New Tool to Perform End-State Free Energy Calculations with GROMACS. J Chem Theory Comput 2021;17:6281–91. https://doi.org/10.1021/acs.jctc.1c00645.

[57] Duan L, Liu X, Zhang JZH. Interaction Entropy: A New Paradigm for Highly Efficient and Reliable Computation of Protein–Ligand Binding Free Energy. J Am Chem Soc 2016;138:5722–8. https://doi.org/10.1021/jacs.6b02682.

[58] Elbahnsi A, Dragomirescu CD, Palumbo N, et al. Mapping the inhibition landscape of P-glycoprotein via conformational ensemble docking. Sci Rep 2026;16:15393. https://doi.org/10.1038/s41598-026-46760-y.